MATCH
Communications in Mathematical and in Computer Chemistry

MATCH Commun. Math. Comput. Chem. **94** (2025) 159–194
ISSN: 0340–6253
doi: 10.46793/match.94-1.159L

Composite Pattern Formation in the Gierer-Meinhardt System with Cross-Diffusion Distributions

Hua Li[a], Min Xiao[a,*], Yonghui Sun[b], Tingwen Huang[c], Jinde Cao[d], Wei Xing Zheng[e]

[a] *College of Automation & College of Artificial Intelligence, Nanjing University of Posts and Telecommunications, Nanjing 210023, China*
[b] *College of Energy and Electrical Engineering, Hohai University, Nanjing 211100, China*
[c] *Faculty of Computer Science and Control Engineering, Shenzhen University of Advanced Technology, Shenzhen 518055, China*
[d] *School of Mathematics, Southeast University, Nanjing 210096, China*
[e] *College of Computer, Data and Mathematical Sciences, Western Sydney University, Sydney, NSW 2751, Australia*

l578109794@163.com, candymanxm2003@aliyun.com, sunyonghui168@163.com, huangtw2024@163.com, jdcao@seu.edu.cn, w.zheng@westernsydney.edu.au

(Received November 18, 2024)

Abstract

The Gierer-Meinhardt system characterizes the fundamental dynamics of pattern formation through the interaction of two variables. Currently, research on the spatiotemporal evolution of this system at home and abroad has been limited to Turing instability and patterns, and research on composite patterns formed by non-uniform cross-diffusion distributions is not yet in-depth. This article presents a composite pattern of the system based on linear, periodic, and

*Corresponding author.

radial distributions of cross diffusion. We conduct a comprehensive study of the two-dimensional spatiotemporal dynamics of the Gierer-Meinhardt model, treating the cross-diffusion coefficients as bifurcation parameters. Using multiscale analysis, the amplitude equation at the Turing threshold is derived. Subsequently, the effects of the proportional-derivative controller, fractional diffusion orders, and anisotropy on system stability, pattern formation, and evolution speed are systematically investigated. Numerical simulations are provided to validate the conclusions.

1 Introduction

In 1952, Turing [1] first used reaction-diffusion equations to describe the mechanisms underlying biological pattern formation on surfaces. Reaction-diffusion systems can describe differential and spatial patterns in biological and chemical fields. Diffusion-induced instability is a key factor driving the formation of spatial patterns. Inspired by Turing's work, reaction-diffusion systems have garnered significant attention, leading to the proposal of numerous models, such as predator-prey models in zoology [2–4], infectious disease models in medicine [5, 6], virus propagation models in cyber-physical systems [7, 8], and various biological and chemical models [9–12]. In 1972, the Gierer-Meinhardt model (GM) was proposed to study molecular mechanisms of catalysis [13]. Gierer and Meinhardt [14] derived the sufficient conditions for spatial pattern formation. Since then, the GM model has been widely used in modeling many biological and chemical reaction processes.

Wu et al. [15] investigated the impact of self-diffusion on the stability of the GM system. They confirmed that self-diffusion could drive Turing instability, which can induce various pattern formations. Ruan [16] considered the GM model for morphogenesis, showing that if the self-diffusion coefficients are appropriately chosen, the uniform equilibrium solution becomes unstable. For the GM system with saturation terms, Song et al. [17] derived the amplitude equations at the bifurcation critical values by using a multi-scale method. Various patterns were obtained through simulation. However, these studies did not consider the role of cross-diffusion on the GM system.

Actually, cross-diffusion can also drive Turing instability [18–21]. Several studies had analyzed the role of cross-diffusion and discussed its impact on pattern formation and pattern types in these systems. Giunta et al. [20] explained that while cross-diffusion coefficients are non-negative in most cases, negative cross-diffusion coefficients also have physical significance in specific biological and chemical systems. Pal et al. [21] stated that negative cross-diffusion coefficients represent a reverse diffusion phenomenon, where the concentration gradient of one substance drives the other substance to diffuse towards the low concentration region. Even if the cross-diffusion coefficient is small or negative, it can still promote pattern formation [22,23]. Lu et al. [24] studied the mechanism of cross-diffusion's impact on spatial patterns in the SI model with nonlinear incidence rates. Dong et al. [25] introduced cross-diffusion into the Schnakenberg system, resulting in temporally periodic patterns, and found that changing the cross-diffusion coefficient could transform these patterns into temporally stable structures. Cross-diffusion also significantly influences the occurrence of supercritical Turing instabilities, as demonstrated by Gambino et al. [26] through weakly nonlinear multi-scale analysis. Notably, there is currently no literature discussing the impact of cross-diffusion on the pattern evolution speed in the GM system.

In the past few years, fractional-order derivatives had been widely incorporated into various models to more accurately describe phenomena [27–31]. Fractional diffusion significantly impacts pattern formation. For instance, Liu et al. [29] investigated Turing instability in a predator-prey system with cross-fractional diffusion. Nec et al. [30] described a superdiffusive resource-consumer system and studied its Turing bifurcation, concluding that fractional diffusion affects the stability of certain equilibria. The impact of cross-fractional diffusio was considered, leading to the study of a predator-prey model [31]. It was ultimately demonstrated that appropriate cross-fractional diffusion can induce Turing patterns. Using fractional-order derivatives provides a better explanation for the pattern formation process in reaction-diffusion systems. Therefore, this paper discusses the impact of fractional diffusion on pattern formation in the GM system.

Control strategies have rapidly advanced and found wide applications across various models [32–36]. The introduction of control strategies significantly impacts various models [37–39]. To date, in order to adapt to the diverse characteristics of systems, an increasing number of control types have emerged [40–42]. There is relatively less research on control strategies for reaction-diffusion systems considering two-dimensional spatial information. Chemical reaction-diffusion systems are characterized by complex spatiotemporal dynamics, where reactant concentrations and diffusion rates are influenced by various factors, leading to instability and pattern changes. The Proportional-Derivative controller (PD), through proportional and derivative control, regulates errors and their rate of change, ensuring a fast response and stability at the desired state. It helps reduce steady-state errors, predicts future changes, and accelerates stabilization, offering precise control over pattern formation and system behavior.

Experimental and theoretical studies have shown that the diffusion processes of many nonlinear physical and biological systems in reality do not conform to the theory of completely random walks. These diffusion processes exhibit directionality, such as anisotropic diffusion in porous media [43], colloids [44], and organ tissues [45]. When randomness and anisotropy are present and a single diffusion direction satisfies the conditions for Turing instability, Turing patterns still exist [46]. The orientation of stripes in Turing patterns is determined by the degree of anisotropic diffusion, and anisotropy enhances the stability of these stripes [47, 48].

This paper considers a GM system with cross-diffusion and extends it to fractional-order diffusion. The effects of cross-diffusion coefficients and the fractional-order diffusion on the system's pattern dynamics are discussed. Additionally, a PD controller is introduced to regulate the system's pattern formation by comprehensively adjusting the controller parameters. Furthermore, the impact of anisotropic diffusion on the system's Turing patterns is also investigated.

2 Model description

This section introduces a fractional order diffusion GM model with cross-diffusion and PD control. Let the concentrations of the activator and inhibitor be represented by u and v, respectively.. Song et al. [17] first proposed the following self-diffusion system:

$$\begin{aligned} \frac{\partial u}{\partial t} =& D_u \nabla^2 u + r\left(\frac{u^2}{(1+pu^2)v} - cu\right), \\ \frac{\partial v}{\partial t} =& D_v \nabla^2 v + r(u^2 - av), \end{aligned} \tag{1}$$

and

$$\nabla^2 = \frac{\partial^2}{\partial x^2} + \frac{\partial^2}{\partial y^2}, \quad (x, y) \in \Omega = [0, R] \times [0, R],$$

where ∇^2 represents the Laplacian operator in a two-dimensional plane, and Ω denotes an internally connected region with a smooth boundary $\partial\Omega$. System (1) follows Neumann boundary conditions

$$\frac{\partial u}{\partial \vartheta} = \frac{\partial v}{\partial \vartheta} = 0,$$

and ϑ represents the unit outward normal vector on the boundary $\partial\Omega$. r is the chemical reaction factor, p is the saturation coefficient. a and c are the degradation rates of the inhibitor and activator, respectively. D_u and D_v are the self-diffusion coefficients. The ordinary differential equation corresponding to system (1) is:

$$\begin{aligned} \frac{\mathrm{d}u}{\mathrm{d}t} =& r\left(\frac{u^2}{(1+pu^2)v} - cu\right), \\ \frac{\mathrm{d}v}{\mathrm{d}t} =& r(u^2 - av). \end{aligned} \tag{2}$$

Except for the origin, the system (2) has a non-trivial equilibrium point $E^* = (u^*, v^*)$, and E^* satisfies

$$\frac{1}{1+p(u^*)^2} = \frac{cu^*}{a}, \; v^* = \frac{(u^*)^2}{a}.$$

Furthermore, to regulate the spatial dynamics of the system, we introduce a PD controller:

$$\eta = K_p e(t) + K_d \frac{\mathrm{d}e}{\mathrm{d}t},$$

where $e(t) = v(t) - v^*$ is the error term, representing the difference between the current state $v(t)$ and the desired target state v^* of the system. The parameter K_p represents the proportional part of the error. A higher value of K_p means that the system responds more aggressively to deviations from the target state. K_p adjusts the response based on the distance between the current state and the desired state. The parameter K_d represents the rate of change of the error, accounting for how fast the error is changing. A higher value of K_d allows the system to predict and react to future changes in the error. The range of the controller coefficients K_p and K_d is flexible, allowing both positive and negative values depending on the desired system behavior and stability requirements [35, 36]. We can get:

$$\begin{aligned} \frac{\mathrm{d}u}{\mathrm{d}t} =& r\left(\frac{u^2}{(1+pu^2)v} - cu\right), \\ \frac{\mathrm{d}v}{\mathrm{d}t} =& r(u^2 - av) + \eta. \end{aligned} \tag{3}$$

The equivalent form of system (3) is :

$$\begin{aligned} \frac{\mathrm{d}u}{\mathrm{d}t} =& r\left(\frac{u^2}{(1+pu^2)v} - cu\right), \\ \frac{\mathrm{d}v}{\mathrm{d}t} =& \frac{r(u^2 - av) + K_p\,(v - v^*)}{1 - K_d}. \end{aligned} \tag{4}$$

Remark. Considering the structure of system (4), its equilibrium point will not change. Consequently, the PD controller can effectively modulate the system's dynamic characteristics while preserving its original equilibrium point E^*.

In chemical catalytic reactions, fractional-order diffusion is utilized as a more appropriate way to describe certain scenarios of catalytic reactions. Research indicates that cross-diffusion can impact the spatiotemporal dynamics of reaction-diffusion systems, affecting phenomena such as pattern

formation and evolutionary rates. To more accurately describe the reaction processes of activators and inhibitors in spatial regions, we introduce cross-diffusion terms in system (4) and extend the diffusion terms to fractional order, resulting in the following form of reaction-diffusion equations:

$$\begin{aligned} \frac{\partial u}{\partial t} =& D_u \nabla^\alpha u + D_{uv} \nabla^\alpha v + r\left(\frac{u^2}{(1+pu^2)v} - cu\right), \\ \frac{\partial v}{\partial t} =& D_{vu} \nabla^\alpha u + D_v \nabla^\alpha v + \frac{r(u^2 - av) + K_p\,(v - v^*)}{1 - K_d}, \end{aligned} \tag{5}$$

where D_{uv} and D_{vu} are the cross-diffusion coefficients. The spectrum definition of the fractional-order diffusion operator $\nabla^\alpha u(x)$ is given by:

$$\nabla^\alpha u\,(x) = -\sum_{j=0}^{\infty} \hat{u}_j \lambda_j^{\frac{\alpha}{2}} \varphi_j,\ u \in I_\alpha,$$

where $I_\alpha = \left\{u = \sum_{j=0}^{\infty} \hat{u}_j \varphi_j, \hat{u}_j = \langle u, \varphi_j \rangle, \sum_{j=0}^{\infty} |\hat{u}_j|^2 |\lambda_j|^{\frac{\alpha}{2}} < \infty\right\}$, λ_j and φ_j are respectively the eigenvalues and orthogonal eigenfunctions of the standard Laplacian operator ∇^2 on a bounded region Ω, satisfying the standard boundary conditions, namely, $\nabla^2 \varphi_j = -\lambda_j \varphi_j$.

Remark. Cross-diffusion models the mutual diffusion between substances, especially when reactant-product interactions are involved [20]. It captures the effects of concentration gradients on diffusion, influencing stability and pattern formation [24, 25] . The advantage of cross-diffusion is its ability to more accurately represent the coupling between substances in complex, heterogeneous environments, offering a more flexible approach compared to self-diffusion models.

Remark. Integer-order diffusion assumes a constant rate and independent behavior, suitable for simple diffusion in homogeneous media. In contrast, fractional-order diffusion can model diffusion in heterogeneous media, capturing changes in the medium's structure and describing non-uniform diffusion in complex media [29, 30].

3 Stability analysis of non-spatial diffusion models

Consider the ordinary differential system (4). Taking into account the practical significance, we focus on the equilibrium point E^* of system (4). The corresponding Jacobian matrix is:

$$J = \begin{pmatrix} J_{11} & J_{12} \\ J_{21} & J_{22} \end{pmatrix} = \begin{pmatrix} rc\left(\frac{2cu^*}{a} - 1\right) & -r\frac{ac}{u^*} \\ \frac{2ru^*}{(1-K_d)} & \frac{-ar+K_p}{1-K_d} \end{pmatrix}.$$

We get the characteristic equation:

$$\lambda_0{}^2 - M_1\lambda_0 + M_2 = 0, \tag{6}$$

where

$$M_1 = J_{11} + J_{22},\ M_2 = J_{11}J_{22} - J_{12}J_{21}.$$

We propose the following hypotheses:

$$(H_1):\ M_1 < 0,\ M_2 > 0.$$

Theorem 1. *If* (H_1) *holds, system* (4) *is locally asymptotically stable at* E^*.

Proof. If (H_1) holds, according to the Routh-Hurwitz criterion, it can be determined that system (4) is locally asymptotically stable at E^*.

Remark. Turing instability is fundamentally caused by diffusion-induced instability. Therefore, subsequent stability analyses of the system are based on the premise that the non-diffusive system (4) is stable at the point E^*. In this case, it is necessary to ensure that (H_1) always holds.

4 The dynamic behavior of spatial diffusion models

4.1 Turing instability

We guarantee the stability of the non-diffusive system (4) at the point E^*, and then extend the time stability of the uniform steady state to non-uniform perturbations:

$$\begin{pmatrix} u \\ v \end{pmatrix} = \sum_k \begin{pmatrix} u_k \\ v_k \end{pmatrix} e^{(\lambda_k t + ik\cdot r)} + c.c., \tag{7}$$

where λ_k represents the growth rate of perturbations at t. i, k, and $\mathbf{r}$ represent the imaginary unit, wave number, and spatial vectors, respectively, and $c.c.$ is the complex conjugate.

By linearizing system (5) around E^*, we get the following equations:

$$\begin{cases} \dfrac{\partial u}{\partial t} = D_u \nabla^\alpha u + D_{uv} \nabla^\alpha v + J_{11} u + J_{12} v, \\ \dfrac{\partial v}{\partial t} = D_{vu} \nabla^\alpha u + D_v \nabla^\alpha v + J_{21} u + J_{22} v. \end{cases} \tag{8}$$

By substituting *Eq.* (7), we can obtain the characteristic equation:

$$\lambda_k{}^2 - M_3(k^\alpha)\lambda_k + M_4(k^\alpha) = 0, \tag{9}$$

where

$$\begin{aligned} M_3(k^\alpha) &= M_1 - (D_u + D_v)k^\alpha, \\ M_4(k^\alpha) &= (D_u D_v - D_{uv} D_{vu})k^{2\alpha} \\ &\quad + (-D_u J_{22} - D_v J_{11} + D_{vu} J_{12} + D_{uv} J_{21})k^\alpha + M_2. \end{aligned}$$

If (H_1) and $D_u + D_v > 0$ hold, then we have $M_3(k^\alpha) < 0$. In this case, the only way for the occurence of Turing instability is $M_4(k^\alpha) < 0$ for certain values of k. We can ascertain the most critical mode value k_T

for system's response to perturbations as follows:

$$k_T = \left(\frac{D_u J_{22} + D_v J_{11} - D_{vu} J_{12} - D_{uv} J_{21}}{2(D_u D_v - D_{uv} D_{vu})} \right)^{\frac{1}{\alpha}}.$$

Substituting k_T back into $M_4(k^\alpha)$:

$$M_{4\min} = M_4(k^\alpha) = M_2 - \frac{(-D_u J_{22} - D_v J_{11} + D_{vu} J_{12} + D_{uv} J_{21})^2}{4(D_u D_v - D_{uv} D_{vu})}.$$

Fixing the other parameters of system (4), we set the cross-diffusion coefficient D_{vu} as the bifurcation parameter and the critical value D_{vu_T} of Turing bifurcation can be obtained by solviong $M_{4\min} = 0$.

From the above analysis, we propose the following assumption:

$$\begin{aligned}(H_2) : & D_u + D_v > 0,\ D_u D_v - D_{uv} D_{vu} > 0, \\ & - D_u J_{22} - D_v J_{11} + D_{vu} J_{12} + D_{uv} J_{21} < 0, \\ & (D_u J_{22} + D_v J_{11} - D_{vu} J_{12} - D_{uv} J_{21})^2 - 4M_2(D_u D_v - D_{uv} D_{vu}) > 0.\end{aligned}$$

Theorem 2. *If* (H_1) *and* (H_2) *hold, then system* (5) *undergoes Turing instability at the equilibrium point* E^*.

Proof. When (H_1) and (H_2) are satisfied, there exists $k^\alpha > 0$ such that $M_4(k^\alpha) < 0$. In this case, *Eq.* (9) has characteristic roots with positive real parts, then system (5) exhibits Turing instability at E^*.

4.2 Turing pattern's amplitude equation

In this subsection, to rigorously characterize the various types of Turing patterns, we employ the method of multiple scales to derive the amplitude equation for system (5) in the vicinity of the Turing bifurcation point. We select D_{vu} as the bifurcation parameter. By setting $u = u^* + \hat{u}$ and $v = v^* + \hat{v}$, and for notational simplicity, we retain the original variables. Consequently, at the point (u^*, v^*), system (5) can be expressed as:

$$\frac{\partial X}{\partial t} = LX + N, \tag{10}$$

where

$$X = \begin{pmatrix} u \\ v \end{pmatrix},\ L = \begin{pmatrix} D_u\nabla^\alpha + J_{11} & D_{uv}\nabla^\alpha + J_{12} \\ D_{vu}\nabla^\alpha + J_{21} & D_v\nabla^\alpha + J_{22} \end{pmatrix},$$
$$N = \begin{pmatrix} \zeta_{20}u^2 + \zeta_{11}uv + \zeta_{02}v^2 + \zeta_{30}u^3 + \zeta_{21}u^2v + \zeta_{12}uv^2 + \zeta_{03}v^3 \\ \chi_{20}u^2 + \chi_{11}uv + \chi_{02}v^2 + \chi_{30}u^3 + \chi_{21}u^2v + \chi_{12}uv^2 + \chi_{03}v^3 \end{pmatrix},$$

in which

$$\zeta_{20} = \frac{c^2r(4cu^* - 3a)}{a^2},\ \zeta_{02} = \frac{a^2cr}{(u^*)^3},\ \zeta_{21} = \frac{c^2r(3a - 4cu^*)}{a(u^*)^2},\ \zeta_{12} = \frac{2ac^2r}{(u^*)^3},$$
$$\zeta_{11} = \frac{-2c^2r}{u^*},\ \zeta_{30} = \frac{4c^2r(a^2 - 3acu^* + 2c^2(u^*)^2)}{a^3u^*},\ \zeta_{03} = \frac{-a^3cr}{(u^*)^5},$$
$$\chi_{20} = \frac{r}{1 - K_d}, \chi_{02} = \chi_{21} = \chi_{12} = \chi_{11} = \chi_{30} = \chi_{03} = 0.$$

Near the Turing bifurcation critical value, expanding D_{vu}, X and N in terms of the small parameter ε:

$$D_{vu_T} - D_{vu} = \varepsilon d_1 + \varepsilon^2 d_2 + \varepsilon^3 d_3 + o(\varepsilon^3), \tag{11}$$

$$\begin{pmatrix} u \\ v \end{pmatrix} = \varepsilon \begin{pmatrix} u_1 \\ v_1 \end{pmatrix} + \varepsilon^2 \begin{pmatrix} u_2 \\ v_2 \end{pmatrix} + \varepsilon^3 \begin{pmatrix} u_3 \\ v_3 \end{pmatrix} + o\left(\varepsilon^3\right), \tag{12}$$

and

$$N = \varepsilon^2 N_2 + \varepsilon^3 N_3 + o\left(\varepsilon^3\right), \tag{13}$$

where

$$N_2 = \begin{pmatrix} \zeta_{20}u^2 + \zeta_{11}uv + \zeta_{02}v^2 \\ \chi_{20}u^2 + \chi_{11}uv + \chi_{02}v^2 \end{pmatrix},$$
$$N_3 = \begin{pmatrix} \zeta_{30}u^3 + \zeta_{21}u^2v + \zeta_{12}uv^2 + \zeta_{03}v^3 \\ \chi_{30}u^3 + \chi_{21}u^2v + \chi_{12}uv^2 + \chi_{03}v^3 \end{pmatrix}.$$

Simultaneously,

$$L = L_c + (D_{vu_T} - D_{vu})M, \tag{14}$$

where

$$L_c = \begin{pmatrix} D_u\nabla^\alpha + J_{11} & D_{uv}\nabla^\alpha + J_{12} \\ D_{vu_T}\nabla^\alpha + J_{21} & D_v\nabla^\alpha + J_{22} \end{pmatrix}, \; M = \begin{pmatrix} 0 & 0 \\ -\nabla^\alpha & 0 \end{pmatrix}.$$

Separate the dynamical scales of the system by letting $t_1 = \epsilon t$, $t_2 = \epsilon^2 t$ and $t_3 = \epsilon^3 t$, and treat them as mutually independent variables, we obtain the following equation:

$$\frac{\partial}{\partial t} = \varepsilon\frac{\partial}{\partial t_1} + \varepsilon^2\frac{\partial}{\partial t_2} + \varepsilon^3\frac{\partial}{\partial t_3} + o(\varepsilon^3). \tag{15}$$

By rearranging, we obtain:

$$\varepsilon : L_c \begin{pmatrix} u_1 \\ \\ v_1 \end{pmatrix} = \mathbf{0}, \tag{16}$$

$$\varepsilon^2 : L_c \begin{pmatrix} u_2 \\ v_2 \end{pmatrix} = \frac{\partial}{\partial t_1}\begin{pmatrix} u_1 \\ v_1 \end{pmatrix} - d_1 M \begin{pmatrix} u_1 \\ v_1 \end{pmatrix} - N_2, \tag{17}$$

$$\begin{aligned} \varepsilon^3 : L_c \begin{pmatrix} u_3 \\ v_3 \end{pmatrix} =& \frac{\partial}{\partial t_1}\begin{pmatrix} u_2 \\ v_2 \end{pmatrix} + \frac{\partial}{\partial t_2}\begin{pmatrix} u_1 \\ v_1 \end{pmatrix} - d_2 M \begin{pmatrix} u_1 \\ \\ v_1 \end{pmatrix} \\ & - d_1 M \begin{pmatrix} u_2 \\ \\ v_2 \end{pmatrix} - N_3. \end{aligned} \tag{18}$$

At the ε order in *Eq.* (16), L_c functions as the system's linear operator at the critical point D_{vu_T}. The solution of perturbation equations can be described by the modulus which includes three wave vectors called k_1, k_2 and k_3, respectively. Soving *Eq.* (16), we can get

$$\begin{pmatrix} u_1 \\ v_1 \end{pmatrix} = \begin{pmatrix} \beta \\ 1 \end{pmatrix} \left(\sum_{j=1}^{3} W_j \mathrm{e}^{(ik_j \cdot r)} + c.c. \right), j = 1, 2, 3, \tag{19}$$

where *c.c.* denotes the complex conjugate and $r = (x, y)$ stands for the spatial vector. W_j is the amplitude of $\mathrm{e}^{(ik_j \cdot r)}$ and

$$\beta = \frac{D_{uv}k_c^{\alpha} - J_{12}}{J_{11} - D_u k_c^{\alpha}}, |k_j| = k_c, k_c^{\alpha} = k_T^{\alpha}(D_{vu}^T).$$

In accordance with the Fredholm solvability condition, *Eq.* (17) must be orthogonal to the null eigenvector of L_c^+. Here, L_c^+ refers to the adjoint of the operator L_c, with its zero eigenvector given by:

$$\begin{pmatrix} 1 \\ \phi \end{pmatrix} \mathrm{e}^{(ik_j \cdot r)} + c.c., j = 1, 2, 3, \tag{20}$$

where $\phi = \frac{D_u k_c^{\alpha} - J_{11}}{J_{21} - D_{vu}^T k_c^{\alpha}}$. L_c^+ and ε^2 satisfy:

$$(1, \phi) \begin{pmatrix} F_u^j \\ F_v^j \end{pmatrix} = 0, \quad j = 1, 2, 3, \tag{21}$$

in which, F_u^j and F_v^j represent the coefficients in F_u and F_v corresponding to $\mathrm{e}^{(ik_j \cdot r)}$, respectively.

Applying the Fredholm solvability condition to *Eq.* (21), we obtain:

$$\begin{cases} (\beta + \phi)\frac{\partial W_1}{\partial t_1} = d_1 k_c^{\alpha} W_1 + 2(\gamma_1 + \phi\gamma_2)\overline{W}_2\overline{W}_3, \\ (\beta + \phi)\frac{\partial W_2}{\partial t_1} = d_1 k_c^{\alpha} W_2 + 2(\gamma_1 + \phi\gamma_2)\overline{W}_1\overline{W}_3, \\ (\beta + \phi)\frac{\partial W_3}{\partial t_1} = d_1 k_c^{\alpha} W_3 + 2(\gamma_1 + \phi\gamma_2)\overline{W}_1\overline{W}_2, \end{cases} \tag{22}$$

where

$$\begin{cases} \gamma_1 = 2\zeta_{20}\beta^2 + 2\zeta_{11}\beta + 2\zeta_{02}, \\ \gamma_2 = 2\chi_{20}\beta^2 + 2\chi_{11}\beta + 2\chi_{02}. \end{cases}$$

Then, solving *Eq.* (17), we can get:

$$\begin{aligned}\begin{pmatrix} u_2 \\ \\ v_2 \end{pmatrix} = &\begin{pmatrix} U_0 \\ V_0 \end{pmatrix} + \sum_{j=1}^{3} \begin{pmatrix} U_j \\ V_j \end{pmatrix} e^{ik_j \cdot r} + \sum_{j=1}^{3} \begin{pmatrix} U_{jj} \\ V_{jj} \end{pmatrix} e^{i2k_j \cdot r} \\ &+ \begin{pmatrix} U_{12} \\ V_{12} \end{pmatrix} e^{i(k_1 - k_2)\cdot r} + \begin{pmatrix} U_{23} \\ V_{23} \end{pmatrix} e^{i(k_2 - k_3)\cdot r} \\ &+ \begin{pmatrix} U_{31} \\ V_{31} \end{pmatrix} e^{i(k_3 - k_1)\cdot r} + c.c.,\end{aligned} \tag{23}$$

where,

$$\begin{pmatrix} U_0 \\ V_0 \end{pmatrix} = \begin{pmatrix} u_{00} \\ v_{00} \end{pmatrix} (|W_1|^2 + |W_2|^2 + |W_3|^2), U_j = \beta V_j,$$
$$\begin{pmatrix} U_{jj} \\ V_{jj} \end{pmatrix} = \begin{pmatrix} u_{11} \\ v_{11} \end{pmatrix} W_j^2, \ \begin{pmatrix} U_{ij} \\ V_{ij} \end{pmatrix} = \begin{pmatrix} u_* \\ v_* \end{pmatrix} W_i \overline{W}_j.$$

The specific expressions are obtained by the method of undetermined coefficients:

$$\begin{pmatrix} u_{00} \\ v_{00} \end{pmatrix} = \frac{-1}{J_{11}J_{22} - J_{12}J_{21}} \begin{pmatrix} J_{22}\gamma_1 - J_{12}\gamma_2 \\ J_{11}\gamma_2 - J_{21}\gamma_1 \end{pmatrix},$$
$$\begin{pmatrix} u_{11} \\ v_{11} \end{pmatrix} = -\frac{1}{2} \begin{pmatrix} J_{11} - 4D_u k_c^\alpha & J_{12} - 4D_{uv} k_c^\alpha \\ J_{21} - 4D_{vu_T} k_c^\alpha & J_{22} - 4D_v k_c^\alpha \end{pmatrix}^{-1} \begin{pmatrix} \gamma_1 \\ \gamma_2 \end{pmatrix},$$
$$\begin{pmatrix} u_* \\ v_* \end{pmatrix} = -\begin{pmatrix} J_{11} - 3D_u k_c^\alpha & J_{12} - 3D_{uv} k_c^\alpha \\ J_{21} - 3D_{vu_T} k_c^\alpha & J_{22} - 3D_v k_c^\alpha \end{pmatrix}^{-1} \begin{pmatrix} \gamma_1 \\ \gamma_2 \end{pmatrix}.$$

For the third-order terms of ε in *Eq.* (18), using the solvability condi-

tion, the results can be obtained as follows through calculation:

$$\begin{aligned}
(\beta+\phi)(\frac{\partial Y_1}{\partial t_1}+\frac{\partial W_1}{\partial t_2}) =& k_c^{\alpha}(d_2W_1+d_1Y_1)-[(I_1+\phi T_1)|W_1|^2 \\
&+2(\gamma_1+\phi\gamma_2)(\overline{W}_2\overline{Y}_3+\overline{W}_3\overline{Y}_2) \\
&+(I_2+\phi T_2)(|W_2|^2+|W_3|^2)]W_1, \\
(\beta+\phi)(\frac{\partial Y_2}{\partial t_1}+\frac{\partial W_2}{\partial t_2}) =& k_c^{\alpha}(d_2W_2+d_1Y_2)-[(I_1+\phi T_1)|W_2|^2 \\
&+2(\gamma_1+\phi\gamma_2)(\overline{W}_1\overline{Y}_3+\overline{W}_3\overline{Y}_1) \\
&+(I_2+\phi T_2)(|W_1|^2+|W_3|^2)]W_2, \\
(\beta+\phi)(\frac{\partial Y_3}{\partial t_1}+\frac{\partial W_3}{\partial t_2}) =& k_c^{\alpha}(d_2W_3+d_1Y_3)-[(I_1+\phi T_1)|W_3|^2 \\
&+2(\gamma_1+\phi\gamma_2)(\overline{W}_2\overline{Y}_1+\overline{W}_1\overline{Y}_2) \\
&+(I_2+\phi T_2)(|W_2|^2+|W_1|^2)]W_3,
\end{aligned} \tag{24}$$

where

$$\begin{aligned}
I_1 =& -(2\beta\zeta_{20}+\zeta_{11})(u_{00}+u_{11})-(\beta\zeta_{11}+2\zeta_{02})(v_{00}+v_{11}) \\
&-3\zeta_{30}\beta^3-3\zeta_{03}-3\zeta_{21}\beta^2-3\zeta_{12}\beta, \\
I_2 =& -(2\beta\zeta_{20}+\zeta_{11})(u_{00}+u_*)-(\beta\zeta_{11}+2\zeta_{02})(v_{00}+v_*) \\
&-6\zeta_{30}\beta^3-6\zeta_{03}-6\zeta_{21}\beta^2-6\zeta_{12}\beta, \\
T_1 =& -(2\beta\chi_{20})(u_{00}+u_{11}), \\
T_2 =& -(2\beta\chi_{20})(u_{00}+u_*).
\end{aligned}$$

The amplitude A_j satisfy the following equation:

$$A_j=\varepsilon W_j+\varepsilon^2Y_j+O\left(\varepsilon^2\right). \tag{25}$$

Eqs. (22) and (24) are multiplied by ε^2 and ε^3, respectively. By utilizing

Eq. (25) to combine these variables, we can obtain the equations:

$$\begin{aligned}
\tau_0\frac{\partial A_1}{\partial t} &= \mu A_1 + g_0\bar{A}_2\bar{A}_3 - [g_1|A_1|^2 + g_2(|A_2|^2 + |A_3|^2)]A_1,\\
\tau_0\frac{\partial A_2}{\partial t} &= \mu A_2 + g_0\bar{A}_1\bar{A}_3 - [g_1|A_2|^2 + g_2(|A_1|^2 + |A_3|^2)]A_2,\\
\tau_0\frac{\partial A_3}{\partial t} &= \mu A_3 + g_0\overline{A}_1\overline{A}_2 - [g_1|A_3|^2 + g_2(|A_1|^2 + |A_2|^2)]A_3,
\end{aligned} \tag{26}$$

where

$$\begin{aligned}
&\tau_0 = \frac{\beta+\phi}{D_{vu_T}k_c^\alpha},\ \mu = \frac{D_{vu_T}-D_{vu}}{D_{vu_T}},\ g_0 = \frac{2(\gamma_1+\phi\gamma_2)}{D_{vu_T}k_c^\alpha},\\
&g_1 = \frac{I_1+\phi T_1}{D_{vu_T}k_c^\alpha},\ g_2 = \frac{I_2+\phi T_2}{D_{vu_T}k_c^\alpha}.
\end{aligned}$$

4.3 Turing pattern stability analysis

By substituting $A_j = \rho_j e^{i\theta_j}$ into *Eq.* (26), we can obtain four different equations:

$$\begin{aligned}
\tau_0\frac{\partial\theta}{\partial t} &= -g_0\frac{\rho_1^2\rho_2^2+\rho_2^2\rho_3^2+\rho_1^2\rho_3^2}{\rho_1\rho_2\rho_3}\sin\theta,\\
\tau_0\frac{\partial\rho_1}{\partial t} &= \mu\rho_1 + |g_0|\,\rho_2\rho_3\cos\theta - g_1\rho_1^3 - g_2\left(\rho_2^2+\rho_3^2\right)\rho_1,\\
\tau_0\frac{\partial\rho_2}{\partial t} &= \mu\rho_2 + |g_0|\,\rho_1\rho_3\cos\theta - g_1\rho_2^3 - g_2\left(\rho_1^2+\rho_3^2\right)\rho_2,\\
\tau_0\frac{\partial\rho_3}{\partial t} &= \mu\rho_3 + |g_0|\,\rho_1\rho_2\cos\theta - g_1\rho_3^3 - g_2\left(\rho_1^2+\rho_2^2\right)\rho_3,
\end{aligned} \tag{27}$$

where $\theta = \theta_1 + \theta_2 + \theta_3$. The following points are summarized:

(1) The uniform states:

$$\rho_1 = \rho_2 = \rho_3 = 0.$$

System (5) is stable for $\mu < \mu_2 = 0$ and unstable for $\mu > \mu_2 = 0$.

(2) The stripe pattern state:

$$\rho_1 = \sqrt{\frac{\mu}{g_1}} \neq 0,\ \rho_2 = \rho_3 = 0.$$

System (5) is stable for $\mu > \mu_3 = \frac{g_0^2 g_1}{(g_2-g_1)^2}$ and unstable $\mu < \mu_3$.

(3) The hexagon pattern or the spot pattern state has the following form:

$$\rho_1 = \rho_2 = \rho_3 = \frac{|g_0| \pm \sqrt{g_0^2 + 4(g_1 + 2g_2)\mu}}{2(g_1 + 2g_2)}.$$

This solution exists when the following condition is satisfied:

$$\mu > \mu_1 = -\frac{g_0^2}{4(g_1 + 2g_2)}.$$

The solution $\rho^- = \frac{|g_0| - \sqrt{g_0^2 + 4(g_1+2g_2)\mu}}{2(g_1+2g_2)}$ is always unstable, and the solution $\rho^+ = \frac{|g_0| + \sqrt{g_0^2 + 4(g_1+2g_2)\mu}}{2(g_1+2g_2)}$ is stable only for

$$\mu < \mu_4 = \frac{g_0^2(2g_1 + g_2)}{(g_2 - g_1)^2}.$$

(4) The mixed state:

$$\rho_1 = \frac{|g_0|}{g_2 - g_1},\ \rho_2 = \rho_3 = \sqrt{\frac{\mu - g_1\rho_1^2}{g_1 + g_2}},$$

where $g_2 > g_1$, and the solution exists when $\mu > \mu_3 = \frac{g_0^2 g_1}{(g_2 - g_1)^2}$. It is always unstable.

5 Numerical simulation

In this section, we conduct a numerical simulation of system (5) in the two-dimensional plane to investigate the formation of two-dimensional patterns. All numerical simulations are performed within $\Omega = (0, 200) \times (0, 200)$, with spatial step sizes $\Delta x = \Delta y = 1$ and a time step size of $\Delta t = 0.05$. Neumann boundary conditions are used. Since the spatial distributions of the activator and inhibitor are similar, we only focus on the formation of spatial patterns of the activator u in the following numerical simulations.

Fix some parameter values of system (5): $a = 0.9$, $c = 1.0$, $r = 0.5$, $p =$

0.1451, $D_u = 0.1$, $D_v = 2.0$ and $D_{uv} = 0.2$. We can obtain $E^* = (u^*, v^*) = (0.820, 0.747)$.

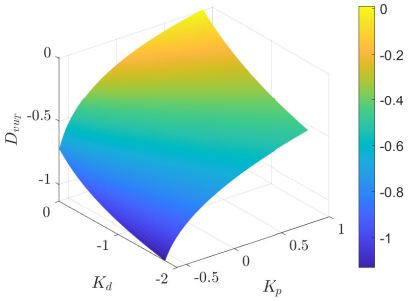

Figure 1. Graph of Turing bifurcation threshold D_{vu_T} varying with control parameter K_p and K_d.

Fig. 1 gives the dependence of D_{vu_T} on the control parameter K_d and K_p for system (5). It can be observed that within a certain range, D_{vu_T} changes as K_p and K_d change.

Remark. We can change the stability of system (5) by adjusting the PD control parameters K_p and K_d. Based on Fig. 1, we discuss the effects of cross-diffusion coefficients, proportional control coefficients, and differential control coefficients on the Turing patterns.

5.1 Influence of the cross-diffusion coefficient D_{vu} on pattern formation

This subsection demonstrates the pattern dynamics corresponding to the values of D_{vu} selected near the critical point D_{vu_T} where Turing instability occurs. Firstly, we set the parameter value $K_p = K_d = 0$, $\alpha = 2$, and get the Turing bifurcation threshold $D_{vu_T} = -0.199$. The coefficients of the corresponding amplitude equation (27) are: $g_0 = 2.3982$, $g_1 = 46.8737$ and $g_2 = 15.7634$. The critical values for the emergence of various patterns are: $\mu_1 = -0.0183$, $\mu_2 = 0$, $\mu_3 = 0.2785$ and $\mu_4 = 0.6507$.

Fig. 2 presents the bifurcation diagram of the amplitude with respect to D_{vu}, and the corresponding critical value of D_{vu} for Turing instability, spot pattern, stripe pattern are $D_{vu_T} = -0.199, D_{vu_p} = -0.144$ and $D_{vu_q} =$

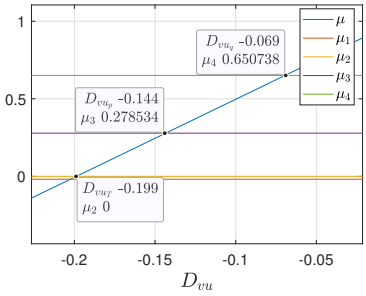

Figure 2. Bifurcation diagram from amplitude equations.

-0.069. Based on these critical values, we select different values of D_{vu} that fall into different regions for simulation.

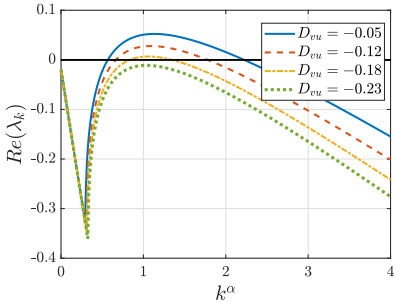

Figure 3. The relationship between $Re\,(\lambda_k)$ about k^α is shown when $D_{vu} = -0.05,\ -0.12,\ -0.18,\ -0.23$.

When $D_{vu} = -0.23 < D_{vu_T}$, system (5) is locally asymptotically stable at E^*. When $D_{vu} = -0.18,\ -0.12,\ -0.05 > D_{vu_T}$, (H_1) and (H_2) hold. According to Theorem 2, system (5) exhibits Turing instability at E^*. Fig. 3 illustrates the relationship between the real part of the eigenvalue $Re\,(\lambda_k)$ and k^α for *Eq.* (9). When $D_{uv} = -0.25$, the characteristic equation (9) has no roots with positive real parts, indicating that system (5) is stable. When $D_{uv} = -0.18$, -0.12, and -0.05, the characteristic equation (9) has roots with positive real parts, implying that system (5) undergoes Turing instability, which is consistent with the previous analysis.

Table 1 calculates the corresponding μ values for the four sets of D_{vu}

and their respective parameter intervals, predicting the resulting pattern formation modes. When $D_{vu} = -0.23$, the corresponding $\mu < \mu_1$. According to theoretical results in subsection 4.3, the system should ultimately be stable. Fig. 4 (a) shows that the system eventually forms a uniform, solid color pattern. When $D_{vu} = -0.18$, the corresponding $\mu \in (\mu_2, \mu_3)$. Fig. 4 (b) shows that the system, after evolution, eventually forms distinct spot patterns. Fig. 4 (c) illustrates the pattern structure corresponding to $D_{vu} = -0.12$; at this point, $\mu \in (\mu_3, \mu_4)$, and the system forms a mixed structure of coexisting spots and stripes. When $D_{vu} = -0.05$, the corresponding $\mu > \mu_4$. Fig. 4 (d) shows that the system ultimately forms only stripe patterns.

Table 1. Coefficients for different parameter values of D_{vu}

D_{vu}	region of D_{vu}	μ	region of μ	Pattern formation
-0.23	$D_{vu}<D_{vu_T}<D_{vu_p}<D_{vu_q}$	-0.157	$\mu<\mu_1<\mu_2<\mu_3<\mu_4$	Steady
-0.18	$D_{vu_T}<D_{vu}<D_{vu_p}<D_{vu_q}$	0.0945	$\mu_1<\mu_2<\mu<\mu_3<\mu_4$	Spot
-0.12	$D_{vu_T}<D_{vu_p}<D_{vu}<D_{vu_q}$	0.3964	$\mu_1<\mu_2<\mu_3<\mu<\mu_4$	Mixed
-0.05	$D_{vu_T}<D_{vu_p}<D_{vu_q}<D_{vu}$	0.7485	$\mu_1<\mu_2<\mu_3<\mu_4<\mu$	Stripe

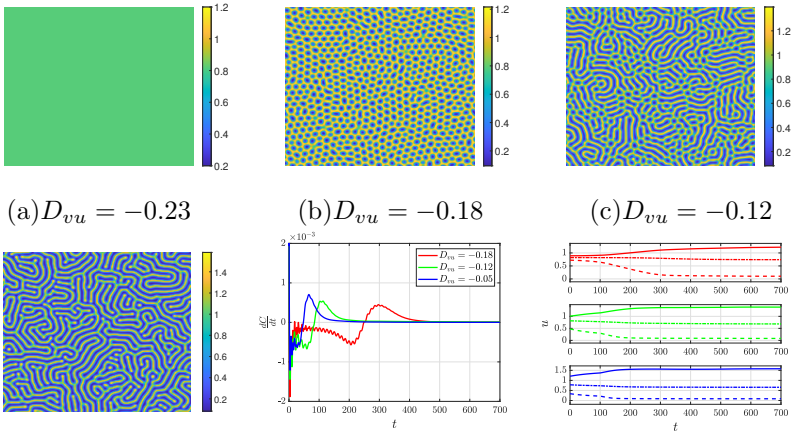

Figure 4. (a)-(d): The pattern structure of system (5) when $D_{vu} = -0.23$, -0.18, -0.12 and -0.05; (e): The time-reciprocal waveform diagram of parameter C; (f): The maximum value, average value, and minimum value of u when $D_{vu} = -0.18, -0.12$ and -0.05.

Remark. Although the emergence of pattern formations is inherently due to the instability of the system, the structure of these patterns eventually stabilizes. To reveal the effect of the cross-diffusion coefficient on the speed of pattern evolution, we construct a lumped parameter using the distribution characteristic parameters at each moment.

By performing a weighted summation of the kurtosis and skewness values at each moment, we obtain the lumped parameter C. During the pattern evolution process, there are usually significant changes in the concentration distribution, leading to noticeable changes in the distribution characteristics of the concentration data. When the system forms a stable pattern mode, the distribution characteristics of the concentration data will no longer change. Therefore, when the lumped parameter C no longer changes, the system has formed a stable pattern mode, and $\frac{dC}{dt}$ approaches 0. The corresponding time t can then be regarded as the time required for the system to form a stable pattern.

Fig. 4 (e) shows the waveform of the $\frac{dC}{dt}$, and Fig. 4 (f) shows the maximum, average, and minimum values of u in the discrete spatial domain at different times, which can be used to describe the time required for the system to form stable patterns. It can be observed that when $D_{vu} = -0.18$, the system requires $t = 500$ to form stable patterns. When $D_{vu} = -0.12$, the system requires $t = 250$ to form stable patterns. When $D_{vu} = -0.05$, the system only needs $t = 150$ to form stable patterns. Therefore, the cross-diffusion coefficient D_{vu} not only changes the system's stable state and pattern structure but also affects the time required for the system to form stable patterns. The larger the absolute value of D_{vu}, the shorter the time required for the system to form patterns.

To more intuitively describe the effect of the cross-diffusion coefficient D_{vu} on the system, we enlarge the reaction domain to $\Omega = (0, 400) \times (0, 400)$ and select D_{vu} as a linear function of the spatial coordinates x

$$D_{vu} = -0.3 + 0.3\frac{x}{400},$$

a periodic function of the spatial coordinates x

$$D_{vu} = -0.15 - 0.15\cos(\frac{10x}{400}),$$

and a spatially varying function of the spatial coordinates x and y

$$D_{vu} = -0.3 + 0.5\frac{\sqrt{(x-200)^2 + (y-200)^2}}{200},$$

for the corresponding simulation experiments.

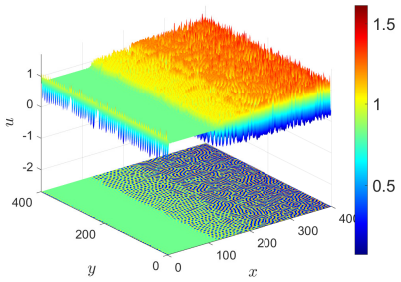

Figure 5. The pattern structure of system (5) when $D_{vu} = -0.3 + 0.3\frac{x}{400}$.

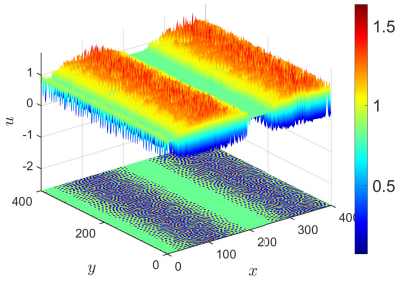

Figure 6. The pattern structure of system (5) when $D_{vu} = -0.15 - 0.15\cos(\frac{10x}{400})$.

Figs. 5-7 show the pattern formations of the system under spatially varying D_{vu}. In Fig. 5, $D_{vu} = -0.3 + 0.3\frac{x}{400}$ varies linearly with x, then $D_{vu} \in (-0.3, 0]$ passes through the three corresponding threshold

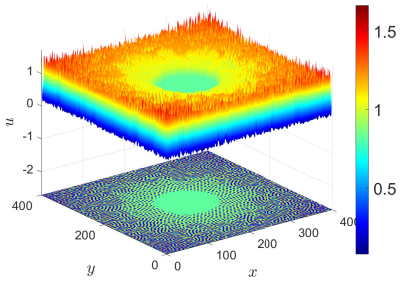

Figure 7. The pattern structure of system (5) when $D_{vu} = -0.3 + 0.5\frac{\sqrt{(x-200)^2+(y-200)^2}}{200}$.

$D_{vu_T} = -0.199, D_{vu_p} = -0.144$ and $D_{vu_q} = -0.069$. As the cross diffusion coefficient D_{vu} increases, the visual pattern undergoes a slow transition from a green solid color pattern to a blue dot pattern on a green background, to the coexistence of blue dots and stripes, and finally becomes a pattern dominated by blue stripes. The patterns change with x, sequentially forming stable patterns, spot patterns, mixed spot-stripe patterns, and stripe patterns. Similarly, in Fig. 6, $D_{vu} = -0.15-0.15\cos(\frac{10x}{400})$ varies periodically with x, then $D_{vu} \in [-0.3, 0]$. The system's patterns also vary periodically with x. In Fig. 7, $D_{vu} = -0.3 + 0.5\frac{\sqrt{(x-200)^2+(y-200)^2}}{200}$ increases radially outward from the center $(200, 200)$. The system exhibits stable patterns, spot patterns, mixed spot-stripe patterns, and stripe patterns from the center outward. We can explain these behaviors by comparing the values of D_{vu} at different locations with the corresponding critical values for Turing instability (D_{vu_T}), spot patterns (D_{vu_p}), and stripe patterns (D_{vu_q}). Therefore, Figs. 5-7 allow us to infer the types of patterns formed under different distributions of D_{vu}.

5.2 Influence of the K_p on pattern formation

This subsection discusses the impact of proportional control coefficients K_p on the pattern dynamics of the system, and $D_{vu} = -0.2$, $K_d = 0$ and $\alpha = 2$ are fixed.

Fig. 8 depicts the dispersion curves of system (5) for different pro-

portional control coefficients K_p. When $K_p = 0.02$, for any k^α, the real parts of the eigenvalues of the characteristic equation (9) are all negative, indicating that the system is stable. For $K_p = -0.06$, -0.15 and -0.2, there is always suitable k^α that makes the real part of the eigenvalues of characteristic equation (9) greater than zero, then the system will generate Turing instability, which verifies Theorem 2.

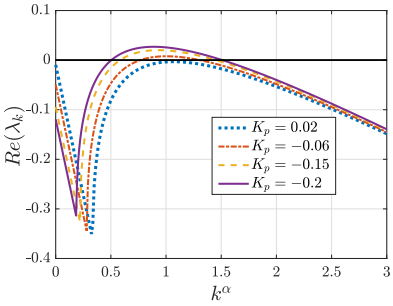

Figure 8. The graphic of $Re(\lambda_k)$ against k^α when $K_p = 0.02,\ -0.06,\ -0.15,\ -0.2$.

Fig. 9 illustrates the pattern evolution process when $K_p = 0.02,\ -0.06,\ -0.15$ and -0.2. When $K_p = 0.02$, system (5) is stable and eventually evolves into a uniform monochromatic distribution. When $K_p = -0.06$, system (5) exhibits Turing instability, resulting in spot patterns. When $K_p = -0.15$, system (5) results in spot-stripe hybrid patterns. When $K_p = -0.2$, system (5) evolves into stripe patterns. From the above simulations, it can be concluded that as the value of K_p changes, system (5) transitions from the local asymptotic stability at the equilibrium point E^* to the Turing instability, and generate different types of patterns.

Similarly, Fig. 9 (e) shows the waveform of the $\frac{dC}{dt}$, and Fig. 9 (f) shows the maximum, average, and minimum values of u in the discrete spatial domain at different times. We can see that when $K_p = -0.06$, the system requires $t = 400$ to form stable patterns. When $K_p = -0.15$, the system requires $t = 250$ to form stable patterns. When $K_p = -0.2$, the system only needs $t = 200$ to form stable patterns. Therefore, the proportional controller parameter K_p can not only change the system's stable state and pattern structure but also affect the time required for the system to form

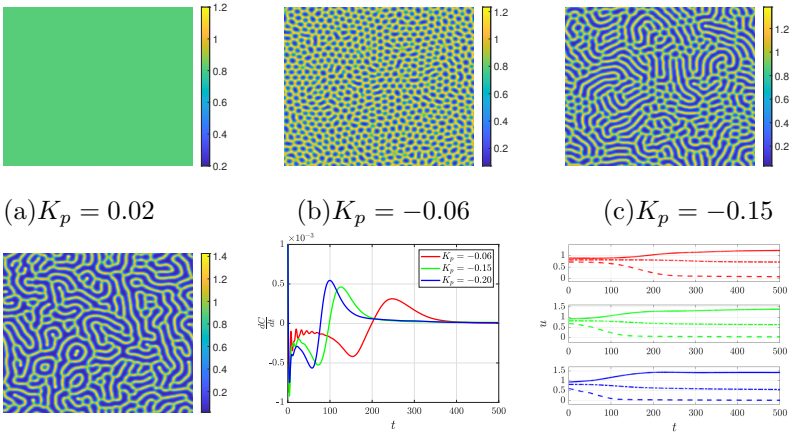

Figure 9. (a)-(d): The pattern structure of system (5) when $K_p = 0.02,\ -0.06,\ -0.15$ and -0.2; (e): The time-reciprocal waveform diagram of parameter C; (f): The maximum value, average value, and minimum value of u when $K_p = -0.06,\ -0.15$ and -0.2.

stable patterns. The larger the value of K_p, the longer the time required for the system to form patterns.

5.3 Influence of the K_d on pattern formation

This subsection discusses the impact of proportional control coefficients K_d on the pattern dynamics of the system, and $D_{vu} = -0.2,\ K_p = 0$ and $\alpha = 2$ are fixed. The analysis process is the same as Subsection 5.2.

Fig. 10 depicts the dispersion curves of system (5) for several differential control coefficients K_d. When $K_d = 0.1$, the real part of the eigenvalues of any k^α characteristic equation (9) is less than zero, so the system is stable. For $K_d = -0.02,\ -0.1$ and -0.3, there is always suitable k^α that makes the real part of the eigenvalues of characteristic equation (9) greater than zero, then the system will generate Turing instability, which verifies Theorem 2.

Fig. 11 illustrates the pattern evolution process when $K_d = 0.1,\ -0.02,\ -0.1$ and -0.3. When $K_d = 0.1$, system (5) is stable. When $K_d = -0.02$,

system (5) resulting in spot patterns. For $K_d = -0.1$, system (5) exhibits spot-stripe hybrid patterns. In contrast, $K_d = -0.3$ leads system (5) to evolve into stripe patterns.

Similarly, we can get that as the value of K_d changes, system (5) transitions from the local asymptotic stability at the equilibrium point E^* to the Turing instability, and generate different types of patterns.

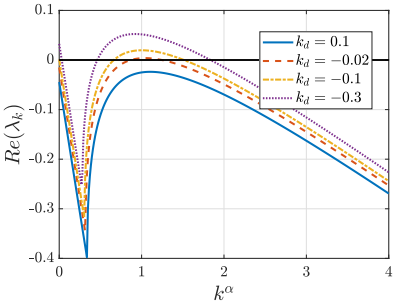

Figure 10. The graphic of $Re(\lambda_k)$ against k^α when $K_d = 0.1$, -0.02, -0.1 and -0.3.

Fig. 11 (e) shows the waveform of the $\frac{dC}{dt}$, and Fig. 11 (f) shows the maximum, average, and minimum values of u in the discrete spatial domain at different times. We get that when $K_d = -0.02$, the system requires $t = 600$ to form stable patterns. When $K_d = -0.1$, the system requires $t = 250$ to form stable patterns. When $K_d = -0.3$, the system only needs $t = 150$ to form stable patterns. Therefore, the differental controller parameter K_d not only changes the system's stable state and pattern structure but also affects the time required for the system to form stable patterns. The larger the value of K_d, the longer the time required for the system to form patterns.

5.4 Influence of the fractional diffusion order α on pattern formation

This subsection discusses the influence of fractional diffusion order α on system pattern dynamics. We set $D_{vu} = -0.2$, $K_p = 0$ and $K_d = 0$.

Fig. 12 reveals that as α increases, the critical wavenumber k_T for

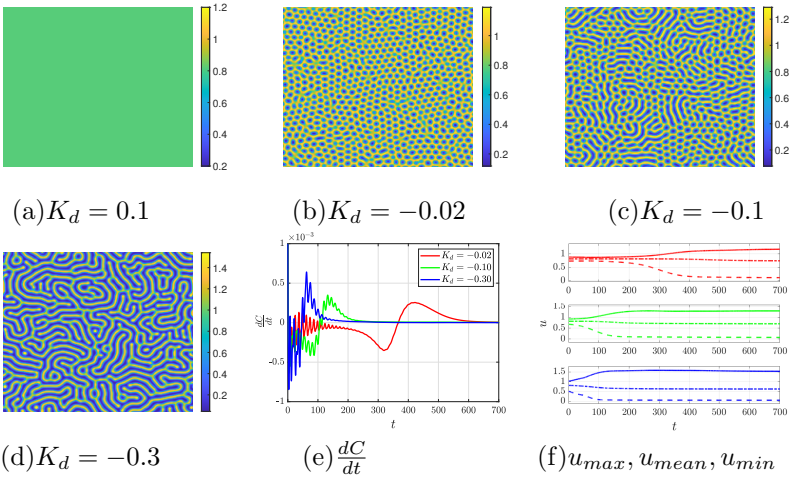

Figure 11. (a)-(d): The pattern structure of system (5) when $K_d = 0.1, -0.02, -0.1$ and -0.3; (e): The time-reciprocal waveform diagram of parameter C; (f): The maximum value, average value, and minimum value of u when $K_d = -0.02, -0.1$ and -0.3.

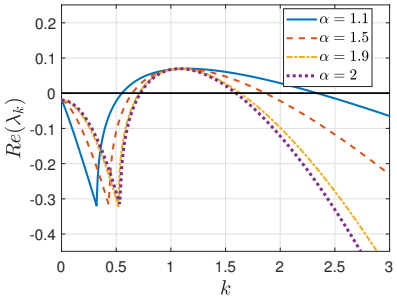

Figure 12. The graphic of $Re(\lambda_k)$ against k when $\alpha = 1.1, 1.5, 1.9, 2.0$.

Turing instability also increases, leading to a smaller wavelength of the solution and a narrower range of wavenumbers for Turing instability.

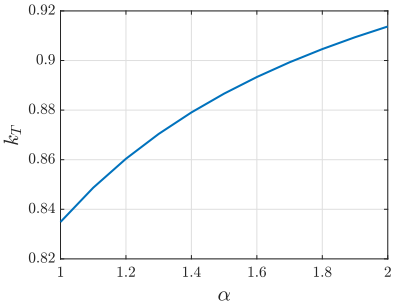

Figure 13. The curve of critical wave number k_T as a function of α.

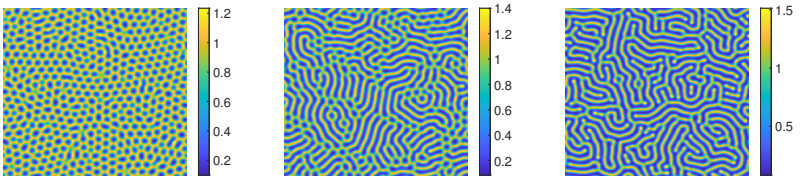

(a)$D_{vu} = -0.18, \alpha = 1.9$ (b)$D_{vu} = -0.12, \alpha = 1.9$ (c)$D_{vu} = -0.05, \alpha = 1.9$

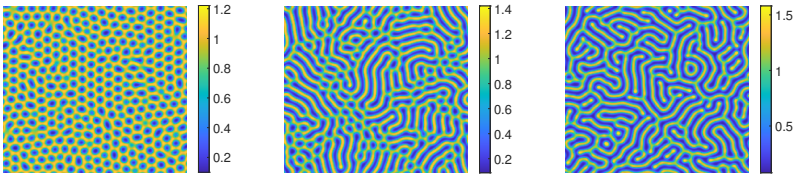

(d)$D_{vu} = -0.18, \alpha = 1.1$ (e)$D_{vu} = -0.12, \alpha = 1.1$ (f)$D_{vu} = -0.05, \alpha = 1.1$

Figure 14. The pattern structure of system (5) for different values of D_{vu} and α.

Fig. 13 provides a more detailed relationship between the critical wavenumber k_T for Turing instability and the fractional diffusion order α. Observing Figs. 14 and 15, we can see that as α increases, the width of the patterns (size of spots and stripes) and the wavelength of the solution all significantly decrease.

Fig. 16 shows the waveform of the $\frac{dC}{dt}$, and Fig. 17 implys the max-

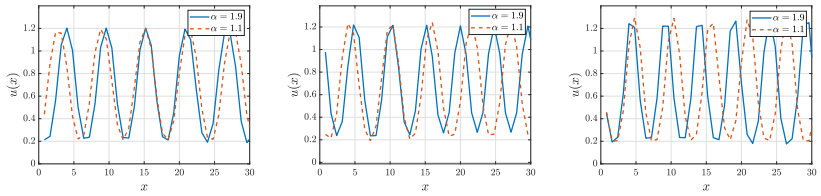

(a)$D_{vu} = -0.18$ (b)$D_{vu} = -0.12$ (c)$D_{vu} = -0.05$

Figure 15. The curve depicting the variation of the wavelength of the solution with respect to α.

imum, average, and minimum values of u in the discrete spatial domain at different times. Differently, The fractional diffusion order α does not affect the time required for the system to form stable patterns.

Remark. The curves for different fractional diffusion orders α are nearly synchronized. This is different from the conclusion regarding the effect of the cross-diffusion coefficient and PD controller on the system's evolution speed.

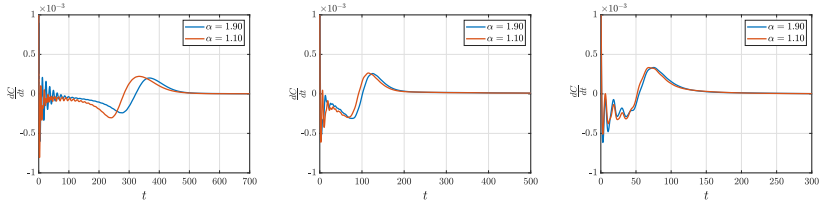

(a)$D_{vu} = -0.18$ (b)$D_{vu} = -0.12$ (c)$D_{vu} = -0.05$

Figure 16. The time-reciprocal waveform diagram of parameter C for different values of D_{vu} and α.

5.5 Influence of the anisotropic diffusion on pattern formation

In this subsection, by keeping $K_p = 0$, $K_d = 0$ and $\alpha = 2$ constant, we study the impact of anisotropic diffusion on Turing patterns by varying the cross-diffusion coefficients D_{vu_x} and D_{vu_y} in different directions. We can obtain the Turing bifurcation threshold $D_{vu_T} = -0.199$. We first fix

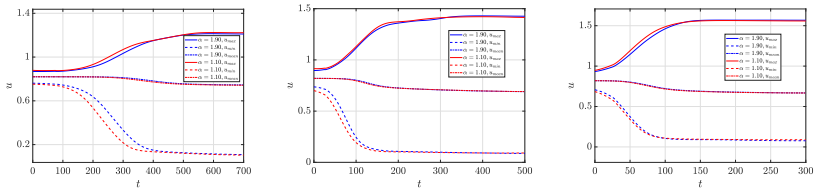

(a)$D_{vu} = -0.18$ (b)$D_{vu} = -0.12$ (c)$D_{vu} = -0.05$

Figure 17. The maximum value, average value, and minimum value of u for different values of D_{vu} and α.

D_{vu_y} while allowing D_{vu_x} to linearly increase in space.

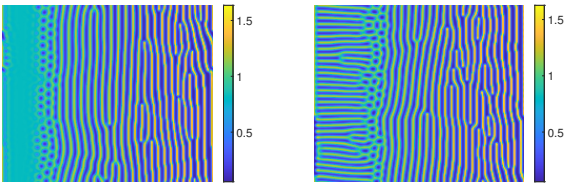

(a)$D_{vu_y} = -0.25$ (b)$D_{vu_y} = -0.18$

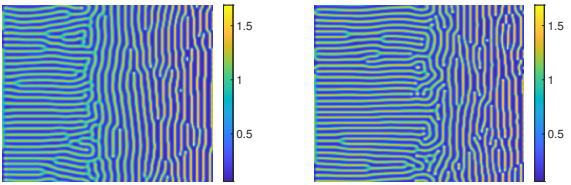

(c)$D_{vu_y} = -0.12$ (d)$D_{vu_y} = -0.05$

Figure 18. When $D_{vu_x} = -0.35 + 0.55\frac{x}{200}$ the pattern structure of system (5).

Fig. 18 illustrates the mixed pattern formed when D_{vu} increases monotonically in the x-direction. As x increases, D_{vu_x} transitions from being lower than D_{vu_y} to gradually becoming higher than D_{vu_y}. For the left part of Fig. 18 (a), where $D_{vu_x} \approx D_{vu_y} = -0.25 < D_{vu_T}$, the system exhibits a stable monochrome state. As D_{vu_x} increases, the following cases occur sequentially: $D_{vu_x} \in (D_{vu_T}, D_{vu_p})$, $D_{vu_x} \in (D_{vu_p}, D_{vu_q})$, and $D_{vu_x} > D_{vu_q}$, corresponding to point, mixed point-stripe, and stripe patterns along the x-direction. However, it is worth noting that because $D_{vu_y} = -0.25 < D_{vu_T}$

remains true, the system is generally stable along the y-direction.

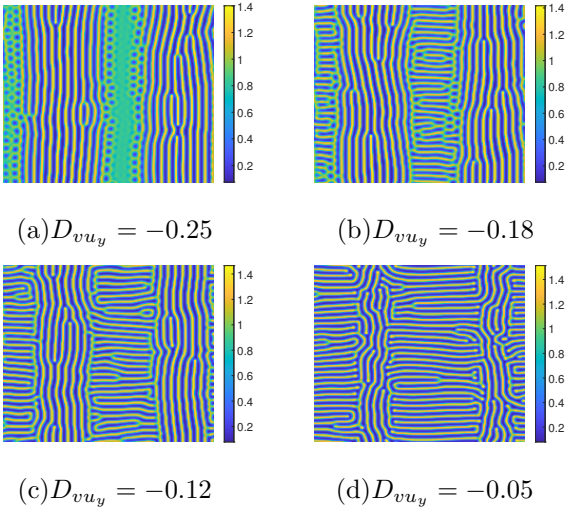

Figure 19. When $D_{vu_x} = -0.15 - 0.15\cos(\frac{10x}{200})$ the pattern structure of system (5).

However, through Fig. 18 (b), (c) and (d), we find that in the left region of these three figures, $D_{vu_x} < D_{vu_y}$, and the system exhibits horizontal stripes. In the right region, $D_{vu_x} > D_{vu_y}$, and the system shows vertical stripes. However, because D_{vu_x} varies linearly with x in all three cases, while their respective D_{vu_y} values are different, larger D_{vu_y} leads to more horizontal stripes.

Similarly, we also provide the system's pattern with D_{vu_x} varying periodically in space as show in Fig. 19, which exhibits phenomena consistent with Fig. 18.

6 Conclusion

This paper derives the conditions for Turing bifurcation in the GM system using cross-diffusion coefficients as bifurcation parameters. Through multi-scale analysis, the amplitude equation at the Turing threshold is derived, predicting the types of patterns that may emerge under different cross-diffusion coefficients. The effects of cross-diffusion coefficients, PD

controllers, and fractional-order diffusion on system stability, pattern formation, and evolution speed are discussed. For the system studied in this article, the findings indicate that the system forms various pattern structures under different cross-diffusion coefficients, with larger cross-diffusion coefficients resulting in shorter times for the system to form stable patterns. When cross-diffusion coefficients are non-uniformly distributed in space, different regions can select different pattern types. The PD controller can alter the Turing bifurcation threshold, affecting the system's stability and the final pattern that evolves. Smaller control coefficients lead to shorter times for the system to achieve stable patterns. Different fractional-order diffusion orders do not affect system stability and evolution speed; however, as the fractional-order diffusion increases, the critical wavenumber for Turing instability also increases, resulting in smaller wavelengths and a higher number of patterns within the same spatial domain. Finally, the impact of anisotropic diffusion on Turing patterns in heterogeneous environments is presented.

***Acknowledgment*:** This work is supported in part by the National Natural Science Foundation of China under Grant 62073172, and the Natural Science Foundation of Jiangsu Province of China under Grant BK20221329.

References

[1] A. M. Turing, The chemical basis of morphogenesis, *Philos. Trans. R. Soc. Lond. B* **237** (1952) 37–72.

[2] M. Chen, R. Wu, Dynamics of a harvested predator–prey model with predator-taxis, *Bull. Malay. Math. Sci. Soc.* **46** (2023) #76.

[3] M. Chen, S. Ham, J. Kim, Taxis-driven complex patterns of a plankton model, *Chaos* **34** (2024) #063101.

[4] M. Chen, R. Wu, Patterns governed by chemotaxis and time delay, *Phys. Rev. E* **109** (2024) #014217.

[5] M. Duan, L. Chang, Z. Jin, Turing patterns of an SI epidemic model with cross-diffusion on complex networks, *Biol. Cybern.* **116** (2022) 501–515.

[6] G. Chen, M. Xiao, Y. H. Wan, X. L. Wang, Propagation dynamics of fractional order delay epidemic model, *Control Theor. Technol.* **38** (2021) 1257–1264.

[7] Q. H. Zhuang, M. Xiao, H. Wang, J. L. Qiu, J. L. Liang, H. J. Jiang, Dynamics of malicious virus propagation in cyber physical systems driven by time-delay and diffusion, *Control Theor. Technol.* **39** (2022) 1407–1415.

[8] L. Wang, M. Xiao, S. Zhou, Y. Z. Zhang, Stability and bifurcation analysis of malicious virus spreading in cyber physical systems under transmission delays, *Control Theor. Technol.* **38** (2021) 81–89.

[9] S. Abdelmalek, S. Bendoukha, The Lengyel-Epstein reaction diffusion system, *Appl. Math. Anal. Theor. Me. Appl.* (2020) 311–351.

[10] A. Giri, J. S. Pramod, S. Kar, Alteration in cross diffusivities governs the nature and dynamics of spatiotemporal pattern formation, *ChemPhysChem* **21** (2020) 1608–1616.

[11] R. Yang, Cross-diffusion induced spatiotemporal patterns in Schnakenberg reaction-diffusion model, *Nonlin. Dyn.* **110** (2022) 1753–1766.

[12] M. Chen, J. Kimb, S. Hamb, Patterns of a general chemical model involving Degn-Harrison reaction scheme, *MATCH Commun. Math. Comput. Chem.* **93** (2025) 267–290.

[13] A. Gierer, H. Meinhardt, A theory of biological pattern formation, *Kybernetik* **12** (1972) 30–39.

[14] A. Gierer, H. Meinhardt, Biological pattern formation involving lateral inhibition, *Lect. Math. Life Sci.* **7** (1974) 163–183.

[15] R. Wu, Y. Zhou, Y. Shao, L. Chen, Bifurcation and Turing patterns of reaction-diffusion activator-inhibitor model, *Phys. A* **482** (2017) 597–610.

[16] S. Ruan, Diffusion-driven instability in the Gierer-Meinhardt model of morphogenesis, *Nat. Resour. Model.* **11** (1998) 131–141.

[17] Y. Song, R. Yang, G. Sun, Pattern dynamics in a Gierer-Meinhardt model with a saturating term, *Appl. Math. Model.* **46** (2017) 476–491.

[18] C. Tian, L. Zhang, Z. Lin, Pattern formation for a model of plankton allelopathy with cross-diffusion, *J. Franklin I* **348** (2024) 1947–1964.

[19] W. Wang, X. Gao, Y. Cai, Turing patterns in a diffusive epidemic model with saturated infection force, *J. Franklin I* **355** (2018) 7226–7245.

[20] G. Giunta, H. Seyed, U. Gerland, Cross-diffusion induced patterns for a single-step enzymatic reaction, *Commun. Phys.* **3** (2020) #167.

[21] D. Pal, D. Kesh, D. Mukherjee, Qualitative study of cross-diffusion and pattern formation in Leslie-Gower predator-prey model with fear and Allee effects, *Chaos Soliton. Fract.* **167** (2023) #113033.

[22] J. Chattopadhyay, P. K. Tapaswi, Effect of cross-diffusion on pattern formation a nonlinear analysis, *Acta Appl. Math.* **48** (1997) 1–12.

[23] V. K. Vanag, I. R. Epstein, Cross-diffusion and pattern formation in reaction-diffusion systems, *Phys. Chem. Chem. Phys.* **11** (2009) 897–912.

[24] Y. S. Lu, M. Xiao, Y. H. Wan, J. Ding, H. J. Jiang, Spatial pattern of a class of SI models driven by cross diffusion, *Acta Phys. Sin.* **73** (2024) #080201.

[25] S. K. Dong, M. Xiao, W. W. Yu, Study on spatiotemporal pattern evolution mechanism of Schnakenberg system, *Acta Autom. Sin.* (2024), **doi:** `https://doi.org/10.16383/j.aas.c230637`

[26] G. Gambino, M. C. Lombardo, S. Lupo, M. Sammartino, Supercritical and sub-critical bifurcations in a reaction-diffusion Schnakenberg model with linear cross-diffusion, *Ric. Mat.* **65** (2016) 449–467.

[27] Z. Liu, Bifurcation anti-control tactics of a fractional-order stable chemical reaction system, *MATCH Commun. Math. Comput. Chem.* **89** (2023) 143–173.

[28] M. A. Khan, Q. Din, Codimension-one and codimension-two bifurcations of a fractional-order cubic autocatalator chemical reaction system, *MATCH Commun. Math. Comput. Chem.* **91** (2024) 415–452.

[29] B. Liu, R. Wu, L. Chen, Patterns induced by super cross-diffusion in a predator-prey system with Michaelis-Menten type harvesting, *Math. Biosci.* **298** (2018) 71–79.

[30] Y. Nec, A. A. Nepomnyashchy, A. A. Golovin, Oscillatory instability in super-diffusive reaction-diffusion systems: Fractional amplitude and phase diffusion equations, *Europhys. Lett.* **82** (2008) #58003.

[31] Z. P. Ma, H. F. Huo, H. Xiang, Spatiotemporal patterns induced by delay and cross-fractional diffusion in a predator-prey model describing intraguild predation, *Math. Method. Appl. Sci.* **43** (2020) 5179–5196.

[32] M. Xiao, W. X. Zheng, J. Lin, Fractional-order PD control at Hopf bifurcations in delayed fractional-order small-world networks, *J. Franklin I* **354** (2017) 7643–7667.

[33] S. Mustafina, E. Antipina, A. Antipin, Solving the optimal control problem with terminal constraints in modeling chemical processes, *MATCH Commun. Math. Comput. Chem.* **91** (2024) 665–682.

[34] C. Xu, M. Liao, M. Farman, Hydrogenolysis of glycerol by heterogeneous catalysis: a fractional order kinetic model with analysis, *MATCH Commun. Math. Comput. Chem.* **91** (2024) 635–664.

[35] Y. F. Luan, M. Xiao, J. Zhao, Bifurcation control of fractional-order hybrid time-delay neural networks based on fractional-order PD control, *Control Theor. Technol.* **30** (2023) 288–98.

[36] P. Zhu, M. Xiao, X. Huang, Spatiotemporal dynamics optimization of a delayed reaction-diffusion mussel-algae model based on PD control strategy, *Chaos, Soliton. Fract.* **173** (2023) #113751.

[37] Y. Lu, Y. Yao, X. Huang X, Investigation of spatial pattern in SI model with PD control and cross-diffusion, *Int. J. Bifurcat. Chaos* (2024) #2450203.

[38] H. Cheng, M. Xiao, W. Yu, L. Rutkowski, J. Cao, How to regulate pattern formations for malware propagation in cyber-physical systems. *Chaos* **34** (2024).

[39] H. He, M. Xiao, Y. Lu, Z. Wang, B. Tao, Control of tipping in a small-world network model via a novel dynamic delayed feedback scheme, *Chaos Soliton. Fract.* **168** (2023) #113171.

[40] M. Xiao, G. Jiang, L. Zhao, State feedback control at Hopf bifurcation in an exponential RED algorithm model, *Nonlin. Dyn.* **76** (2014) 1469–1484.

[41] W. Ren, R. Cheng, H. Ge, Q. Wei, Bifurcation control in an optimal velocity model via double time-delay feedback method, *IEEE Access* **8** (2020) 216162–216175.

[42] M. Peng, Z. Zhang, X. Wang, Hybrid control of Hopf bifurcation in a Lotka-Volterra predator-prey model with two delays, *Adv. Differ. Eq.* **2017** (2017) 1–20.

[43] L. Si, H. Zhang, J. Wei, B. Li, H. Han, Modeling and experiment for effective diffusion coefficient of gas in water-saturated coal, *Fuel* **284** (2021) #118887.

[44] F. J. Lin, J. J. Liao, J. C. Wu, B. Q. Ai, Solid-liquid transition induced by the anisotropic diffusion of colloidal particles, *Chinese Phys. B* **31** (2022) #036401.

[45] F. L. Zhou, D. J. Mchugh, Z. Li, J. E. Gough, G. R. Williams, G. J. Parker, Coaxial electrospun biomimetic copolymer fibres for application in diffusion magnetic resonance imaging, *Bioinspir. Biomim.* **16** (2021) #046016.

[46] D. M. Busiello, G. Planchon, M. Asllani, T. Carletti, D. Fanelli, Pattern formation for reactive species undergoing anisotropic diffusion, *The Eur. Phys. J. B* **88** (2015) 1–7.

[47] H. Shoji, Y. Iwasa, A. Mochizuki, S. Kondo, Directionality of stripes formed by anisotropic reaction-diffusion models, *J. Theor. Biol.* **214** (2002) 549–561.

[48] H. Shoji, A. Mochizuki, Y. Iwasa, M. Hirata, T. Watanabe, S. Hioki, S. Kondo, Origin of directionality in the fish stripe pattern, *Dev. Dyn.* **226** (2003) 627–633.